KATJA WAETZIG (Orcid ID : 0000-0003-2606-8065)

JOCHEN SCHILM (Orcid ID : 0000-0002-8190-6933)

Article type : Research Article

Electronic, mechanical, and thermal properties of $[Ca_{24}Al_{28}O_{64}]^{4+}(4e^-)$ electride ceramic

Katja Waetzig*, Jochen Schilm

Fraunhofer IKTS, Institute for Ceramic Technologies and Systems, Winterbergstraße 24, Dresden, Germany.

* corresponding author: katja.waetzig@ikts.fraunhofer.de

Abstract

The compound $[Ca_{24}Al_{28}O_{64}]^{4+}(4e-)$ named as C12A7:e- has outstanding properties because of a low work function and high electron conductivity due to a cage like crystal structure. For the application of the material as hollow cathodes in small satellite propulsion systems, its preparation as sinterable glass ceramics via the powder route is purposeful. However, the mechanical and thermal properties of the C12A7:e- glass ceramics have only been insufficiently measured so far. In this study, the measured Vickers hardness (HV0.5) is 6.7 ± 0.2 GPa. The ceramic has a fracture toughness of 1.6 MPa $m^{0.5}$ (calculated by Shetty model) and a 4-pt. bending strength of σ = 75 ± 12 MPa (σ_0 = 90 MPa). The coefficient of thermal expansion CTE is between 4.2 and 6.0 × 10^{-6} K^{-1} (RT-1000 °C) and the thermal conductivity ranges between 2.3 W m^{-1} K^{-1} (20 °C) and 1.7 W m^{-1} K^{-1} (1000 °C). For calculating the thermal conductivity, the heat capacity and the thermal diffusivity are measured.

Keywords

electride, C12A7, $12CaO{\cdot}7Al_2O_3$, $[Ca_{24}Al_{28}O_{64}]^{4+}(4e^-)$, glass ceramic, hardness, toughness, strength, thermal expansion coefficient, CTE, heat capacity, thermal conductivity

Introduction

The compound $12CaO{\cdot}7Al_2O_3$ (C12A7, $Ca_{12}Al_{14}O_{33}$) is formed near the eutectic composition in the $CaO\text{-}Al_2O_3$ system in the temperature range between ~850 °C and the melting point of ~1410 °C [1] (Fig. 1). This rather rare circumstance makes it possible to synthesize this composition via the melt as a glass or glass frit. Powders prepared from such glass frits, respectively, powder compacts made thereof can be transferred into dense polycrystalline glass ceramic microstructures by a combined sintering and crystallization step [2]. Other methods for the preparation of the crystalline compound can be either the growth as a single crystal [3,4], sintering as polycrystalline ceramic [5], plasma arc melting [6] or deposition as thin film [7]. By the cage structure a positively charged framework $[Ca_{24}Al_{28}O_{64}]^{4+}$ is built, in which the charge balance can be given by two O^{2-} (oxide), four e^- (electride), four H^- (hydride) or other anions such as Cl^- [8,9,10].

In case of the electron-occupied composition $[Ca_{24}Al_{28}O_{64}]^{4+}(4e^-)$ - also named as C12A7:e- in the following - the known electronic properties are characterized for several different preparation routes (Tab. 1). For C12A7:e- single crystals highest electronic conductivity is ranging between 100 and 1500 $S\,cm^{-1}$ and also highest electron concentrations (electron density) of about 2×10^{21} cm^{-3} are determined by optical absorption [11,12,13,14]. In comparison to the single crystalline C12A7:e-, the polycrystalline ceramics seem to indicate a lower conductivity along with a decreased electron concentration [15,16]. But the differences in the single and polycrystalline structure do not exclusively explain these lower values but also the measuring method used for determining the electron concentration. Using electron paramagnetic resonance (EPR) for determination of the electron concentration is not comparable to optical absorption, because the saturated diamagnetic electron pairs are not distributing on the measured signal [17,18]. Similar is the situation with Hall measurement, which detects only the mobile electrons [16]. So, the reported data on the electronic properties summarized in table 1 do not allow a direct comparison or a reliable characterization but give a profound base for the explanation of the unique properties of this material.

Table 1 Overview of the properties of C12A7:e- electride (RT = room temperature):

C12A7 material	**preparation**	**electronic properties**	**mechanical, thermal properties**	**reference**
single crystal	growing of crystals and	electron concentration:	not reported	H. Hosono, 2004 [11];

	reduction with Ca metal vapor	~2 x 10^{21} cm^{-3} (1); conductivity at RT: ~100 S cm^{-1}		S.-W. Kim, 2007 [5]; S. Matsuishi, 2003 [12]
		electron concentration: ~2 x 10^{21} cm^{-3} (1); conductivity at RT: ~800 S cm^{-1}	not reported	Y. Toda, 2011 [13]
single crystal	growing of crystals and reduction with Ti metal vapor	electron concentration: 2.3 x 10^{21} cm^{-3} (1); ~1500 S cm^{-1}	not reported	R. P. S. M. Lobo, 2015 [14]
single crystal	growing of crystals and reduction in graphite crucible T = 1200 °C for 24 h	electron concentration: 8 x 10^{19} cm^{-3} (2); conductivity at RT: ~4 S cm^{-1}	not reported	S.-W. Kim et al., 2006 [15]
glass-ceramic	solidification of glass melt, crystallization, and reduction under vacuum	electron concentration: 1 x 10^{19} ~ 3 x 10^{19} cm^{-3} (2)	not reported	S.-W. Kim, 2007 [5]
ceramic	pre-sintered ceramic and reduction with Ti metal vapor	electron concentration: 5.9 x 10^{19} cm^{-3} (3); conductivity at RT: 142 S cm^{-1}	not reported	J. Zhao, 2018 [16]
ceramic	sintering with Al metal for reduction by spark plasma sintering (SPS)	electron concentration: 2.3 x 10^{21} cm^{-3} (1) 1 x 10^{18} cm^{-3} (2)	not reported	F. Li, 2018 [17]
ceramic	spark plasma sintering (SPS)	electron concentration: 2 x 10^{21} cm^{-3} (1) 6.3 x 10^{19} cm^{-3} (2); conductivity at RT: 1136 S cm^{-1}	not reported	Y. Xiao, 2020 [18]
ceramic	sintering in carbon at T = 1300 °C (not completely reduced)	not reported	thermal conductivity: 1.34-1.66 W m^{-1} K^{-1} (RT-250 °C)	C. Rudradawong, 2019 [19]
ceramic	sintering in graphite crucible at T = 1430 °C	not reported	thermal conductivity: 1.9-3.1 W m^{-1} K^{-1} (RT-	J. Mackey, 2020 [20]

			600 °C); CTE: 7 x 10^{-6} K^{-1}	

Methods for measuring the electron concentration: (1) UV absorption, (2) electron paramagnetic resonance (EPR) or electron spin resonance (ESR), (3) Hall measurement.

Even less reported than data on the electronic properties are those on the thermal and mechanical properties of C12A7:e- ceramic. For the oxide C12A7, a thermal conductivity of 1.7-1.3 W m^{-1} K^{-1} (RT-250 °C) was measured by Rudradawong et al. [19]. A slightly higher value of 3.1-1.9 W m^{-1} K^{-1} (RT-600 °C) is reported by Mackey et al. [20] for the C12A7:e- electride ceramic. In the same paper, the coefficient of thermal expansion (CTE) is given as 7 x 10^{-6} K^{-1}.

In this study, the C12A7:e- material was prepared by a glass ceramic route and samples were prepared by sintering under nitrogen in a graphite crucible. Details of the synthesis procedure have been published earlier [2]. For measuring the electronic, thermal, and mechanical properties, different specimen geometries were cut and dry ground. With this the electron concentration, the thermal conductivity, diffusivity, and the coefficient of thermal expansion as well as the hardness, fracture toughness and bending strength were determined.

Experimental

To prepare C12A7 oxide powder, $CaCO_3$ (VWR Chemicals) and Al_2O_3 (NABALOX®, Nabaltec) were first mixed with stoichiometric ratio of 12:7 in a tumbling mixer. This mixture was melted in a platinum crucible by heating in a muffle furnace to a temperature above 1450 °C. The melt was quenched on a brass block and the glass splinters were ground in a rotating disk mill (RS 200, Retsch), in a planetary ball mill (Pulverisette 5, Fritsch) for 12 h and in a vertical ball mill (NETZSCH Feinmahltechnik). The last milling step was performed as wet milling process with ethanol and alumina balls for 2 h.

For measuring the electron density of the resulting electride, the samples must be thinner than 1 mm. Therefore, the prepared oxide powder was casted as slurry with binder, dispersant and plasticizer to a tape. The flexible tape was cutted by Laser into samples with 40 mm x 40 mm dimension. The samples were presintered by debinding and sintering in one step by heating with 0.5 K/min to a temperature of 600 °C and

with 3 K/min to the final temperature of 1200 °C in air. A thermal treatment step under reductive atmosphere, described later in detail, was performed to transform the oxide into the electride.

For specimen with other dimensions for thermal and mechanical testing, the powder compacts were dry-pressed into shape with a pressure of 50 MPa and afterwards cold-isostatically compacted with 700 MPa. All samples made of the tape and after compaction were sintered under reductive atmosphere with 5 K/min heating ramp at a temperature of 1340 °C for 10 h dwell time.

The phase composition of the sintered glass ceramic was characterized using a powder X-ray diffractometer D8 Advance (Ltd.Bruker AXS) using Cu Ka radiation and a LynxEye position sensitive detector. The phase composition was determined by TOPAS software (V5, Ltd., BrukerAXS). The microstructure was visualized after ion beam polishing with a field assisted electron beam source microscope (NVision 40, Zeiss GmbH).

The specific resistance and the electron density (electron concentration) were determined using a Hall measurement system (RH2035, PhysTech GmbH) with van-der-Pauw geometry of the contacted specimen. For contacting the electride ceramic, a silver-based paste was used, and the electron density was measured in a magnetic field of 0.8 T at a temperature of 22 °C.

The electron concentration was measured with a second method by determination of mass changes during oxidation. Therefore, thermogravimetric equipment (STA 449 C, NETZSCH-Gerätebau GmbH) was used for measuring the mass increase in air of a C12A7:e- sample during heating with 5 K/min to a temperature of 1200 °C and electron concentration was calculated.

For measuring the hardness by indentation, the surface of the C12A7:e- ceramic was dry-polished and a standard indenter with a Vickers diamond was used for testing with the XM1280A (Ahotec, Germany). Three testing loads of 49.1 N (HV5), 9.81 N (HV1) and 4.91 N (HV0.5) were applied. Due to the brittleness of the C12A7:e- ceramic, an analysis of the results was only possible when using a load corresponding to HV0.5, and the hardness was calculated as an average of 10 indentations. The crack lengths on the wedges were determined for calculating the toughness K1C with the Shetty equation [21].

For the determination of the strength, more than 10 bending bars with 2.5 mm x 2.5 mm x >25 mm were cut and water-free ground with oil. The 4-point-bending tests were performed using an Inspekt Table 10-1 (Hegewald & Peschke) with 0.5 mm/min speed, 10 mm inner span and 20 mm outer span as described in the german standard DIN EN 843-1:2006. The bending strength was calculated as an average value of 10 specimen.

The coefficient of thermal expansion (CTE) was measured on samples with the dimensions of 4 mm x 4 mm x 20 mm using dilatometry (DIL 402 E, NETZSCH-Gerätebau GmbH). The thermal diffusivity α was measured with the Laser Flash Method (Laser-Flash-Apparatus LFA 427, NETZSCH-Gerätebau GmbH) on cylindrical samples with a diameter of 10 mm and a thickness 1.8 mm and the heat capacity was determined with small samples by Differential Scanning Calorimetry (DSC 404, NETZSCH-Gerätebau GmbH). Finally, the thermal conductivity κ was calculated with equation:

$$\kappa(T) = \alpha(T) \cdot \rho \cdot c_p(T)$$

κ … thermal conductivity, α … thermal diffusivity, ρ … density (C12A7: 2.68 g cm^{-3}), c_p … heat capacity

Results and discussion

Phase composition and microstructure

The phase analysis and the microstructure of the sintered C12A7:e- ceramic are presented in Figure 2. The main phase C12A7 contains small amounts of minor phase C3A ($Ca_3Al_2O_6$) and CA ($CaAl_2O_4$), which is evident in the phase analysis by the marked reflections and in the microstructure by the lighter grains. A heavy phase in the triple points was observed, likely being attrition from WC during grinding of the glass. Since the reflections could not be clearly assigned, their content is assumed to be <1 wt%. Neglecting this phase, the contents of the Ca-Al-O phases were determined as follows: 91.5 wt% C12A7 (Mayenite), 8.2 wt% C3A and 0.3 wt% CA. Due to the ion beam polishing, the grain boundaries are not observable, so that the microstructure has a glassy impression with interruption of some pores and the impurity of the secondary phase. The surface preparation with etching techniques to visualize the grain boundaries was not possible due to the sensitivity to moisture of the etching polish. Thermal etching was also not successful. Therefore, no information of the grain size distribution can be given.

Electronic properties

The C12A7:e- electride with 600 µm thickness was characterized by Hall method (Fig. 3). A specific resistance of 0.14 Ohm cm (conductivity σ of 7.1 S cm^{-1}) and an electron concentration of 4.9 x 10^{18} cm^{-3} are determined. The calculated electron mobility is 9.05 $cm^2V^{-1}s^{-1}$.

On the first view, the measured values seem to be low in comparison to single crystals (2 x 10^{21} cm^{-3}; σ = 100 S cm^{-1}[11]). Kim et al. [15] measured a comparable conductivity (~4 S cm^{-1}) but a higher electron concentration of 8 x 10^{19} cm^{-3} by ESR method for sintered ceramics. Li and Xiao et al. [16,18] used the UV absorption and the ESR method to determine the electron concentration of C12A7:e- ceramics prepared by SPS. With ESR, the electron concentration is in the range between 10^{18} and 10^{19} cm^{-3}, whereas the electron concentration of 2 x 10^{21} cm^{-3} is 2-3 orders of magnitude higher measured by the UV absorption.

The Hall measurement can only detect the mobile electrons. Therefore, the electron concentration of 4.9 x 10^{18} cm^{-3} by Hall method is lower but seems to correlate with data measured by ESR. For this reason, the oxidation behavior was investigated thermogravimetrically on samples examined previously by means of Hall measurement. It can be strongly assumed, that the finally measured mass gain corresponds directly to overall concentration of electrons contained in the C12A7:e- electride. Hence the electrons substituted by O^{2-} result in an electron concentration of 1.0 x 10^{21} cm^{-3} calculated by the mass increase. This value is in the same order of magnitude as data measured by the UV absorption method.

Therefore, the electron concentration measured on C12A7:e- is dependent on the used characterization method. The ESR and Hall method are underestimating the overall electron concentration, as this method can only detect the mobile electrons in the microstructure.

Mechanical properties

For the first time, C12A7:e- electride ceramic were characterized in terms of mechanical properties. For measuring the hardness with Vickers indentation methods, the surface of the ceramics was dry-polished. With a testing load of 49.1 N (HV5), the edge lengths of the indentation were not clearly measurable (Fig. 4a), because of brittle chipping of the ceramic. Therefore, the load was reduced to 9.81 N (HV1) without measurable indentation (Fig. 4b). After reducing the load to 4.91 N (HV0.5), the indentation was measurable (Fig. 4c) and a hardness of 685 ± 17 (6.7 ± 0.2 GPa) is determined. A fracture toughness of 1.6 MPa $m^{0.5}$ was calculated according to the Shetty model [21] using the crack length of the loaded wedges as a mechanical analogue. These low values of hardness and toughness as well as the brittle chipping of the material at the surface indicate a behaviour of the C12A7:e- electride which is more comparable to glass than to a conventional ceramic microstructure. A comprehensible explanation of these properties cannot be provided here, not least because of the limited informative SEM images of the microstructure. Based on these results,

we assume that after crystallization and densification of the parent glass powder compacts into a dense glass ceramic microstructure the glassy properties still predominate the fracture behavior. In a previous study it has been demonstrated that the parent glass crystallizes (accompanied by a volume increase) before the sintering process starts at 1050°C [2]. A strengthening effect caused by the crystalline phases, which is known from other types of glass ceramic materials is not observed.

To determine the 4-point bending strength, 20 bending bars were machined by cutting and dry grinding. Of these, only 10 were tested as they did not show any obvious damage due to chipping. The bending strength of $\sigma = 75 \pm 12$ MPa ($\sigma_0 = 90$ MPa) is also lower than expected for a ceramic material (Fig. 5). Also, this low bending strength indicates a behavior of the C12A7:e- ceramic which is more typical for an oxide glass.

Thermal properties

The coefficient of thermal expansion (CTE) of the C12A7:e- electride ceramic was measured in a temperature range between 25 and 1000 °C in one cycle (Tab. 2, Fig. 6). Starting with 4.2 x 10^{-6} K^{-1} at room temperature, the CTE is increasing to 6.0 x 10^{-6} K^{-1} at T = 1000 °C. Mackey et al. [20] measured a CTE of 6 x 10^{-6} K^{-1} (RT-600 °C) in the 1st cycle and 7 x 10^{-6} K^{-1} (RT-600 °C) in the 2nd cycle for the C12A7:e- electride ceramic.

Table 2 Coefficient of thermal expansion (CTE) of C12A7:e- ceramic:

Temperature [°C]	**CTE 10^{-6} [K^{-1}]**
25	4.2
100	4.6
200	4.9
400	5.3
1000	6.0

To calculate the thermal conductivity, the thermal diffusivity and the heat capacity were determined. Figure 7 is presenting the thermal diffusivity of 1.0 - 0.5 mm^2s^{-1} and heat capacity of 0.8 - 1.1 J g^{-1} K^{-1} for the C12A7:e- ceramic in the temperature range between 25 and 1000 °C.

Starting at 2.3 W m^{-1} K^{-1} (25 °C), the thermal conductivity decreased with increasing temperature to 1.7 W m^{-1} K^{-1} (1000 °C). These values are in between of the thermal conductivity of C12A7 oxide ceramic (1.7-1.3 W m^{-1} K^{-1} (RT-250 °C)) measured by Rudradawong et al. [19] and the data of 3.1-1.9 W m^{-1} K^{-1} (RT-600 °C) for C12A7:e- electride reported by Mackey et al. [20].

In comparison to Mackey et al. [20], our data of CTE and thermal conductivity are slightly lower. Independent of measurement inaccuracies, the composition and the electronic state of the samples could explain the differences in the measurements. Three main differences could be reasonable for influencing the thermal properties: (1) Mackey et al. [20] reported the contamination of the C12A7 with secondary phases ($Ca_3Al_2O_6$, $Ca_5Al_6O_{12}$, and $CaAl_2O_4$), and (2) the occupation with C_2^{2-} ions in the structure of C12A7:e-, additionally, (3) the electronic state (electron density) is not reported. It is possible that these differences in the sample composition led to lower values in our investigation.

The mechanical and thermal properties are influencing the application of C12A7:e- ceramic. The low mechanical properties are complicating the machining of the sintered material without chipping. Additionally, the low thermal conductivity is influencing the measurement of thermionic performance on a heater or overheating by applying a voltage during characterization of the work function.

Conclusion

The $[Ca_{24}Al_{28}O_{64}]^{4+}(4e^-)$ ceramic named as C12A7:e- was characterized regarding its electronic, mechanical, and thermal properties. A specific conductivity σ of 7.1 S cm^{-1} was determined in correlation to an electron concentration of 4.9 x 10^{18} cm^{-3} by Hall measurement and 1.0 x 10^{21} cm^{-3} by oxidation. With the Hall method, only mobile electrons are detected, while the increase in mass due to oxidation reflects the content of all electrons.

The mechanical characterization of the hardness by indentation was difficult because of the chipping of the C12A7:e- under load. Therefore, the low hardness (HV1) of 685 ± 17 (6.7 ± 0.2 GPa), and fracture toughness of 1.6 MPa $m^{0.5}$ were determined. This behavior was also reflected in the production of bending bars for strength determination. Only 10 bending bars had no obvious defects and was tested. The bending strength of σ = 75 ± 12 MPa (σ_0 = 90 MPa) by 4-point-bending test was measured for the C12A7:e- electride ceramic.

Finally, the coefficient of thermal expansion CTE of 4.2 - 6.0 × 10^{-6} K^{-1} (RT-1000 °C) and the thermal conductivity of 2.3 - 1.7 W m^{-1} K^{-1} (RT-1000 °C) were determined.

Acknowledgement

The author thanks I. Eichler and K. Jungnickel for melting C12A7, powder processing; D. Schabbel for tape casting; M. Scholz for sintering; M. Nake and colleagues for preparing the specimen; B. Matthey and colleagues for XRD measurement, phase analysis and quantification; S. Höhn and colleagues for SEM image; M. Trache for Hall measurement; C. Steinborn, A. Bales, and U. Körber for measuring the mechanical properties as well as T. Gestrich and colleagues for measuring the thermal properties as well as A. Post and his colleagues for recommendation of measuring the weight change by oxidation.

This work was supported by the European Union's Horizon 2020 research and innovation programme under grant agreement No 828902 (E.T. PACK project) and grant agreement No 870336 (iFACT project).

Figures and Captions

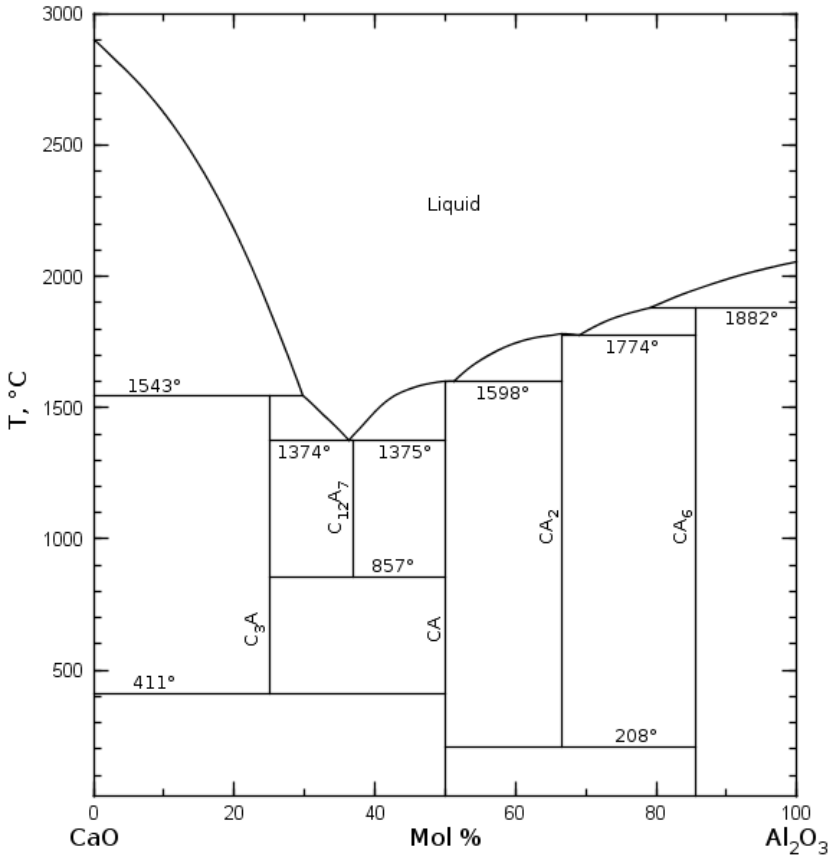

Figure 1

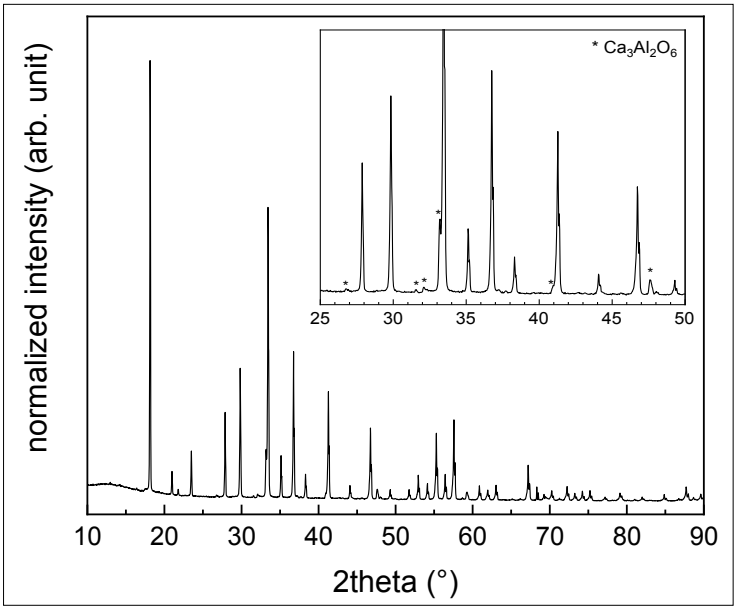

Fig 2a)

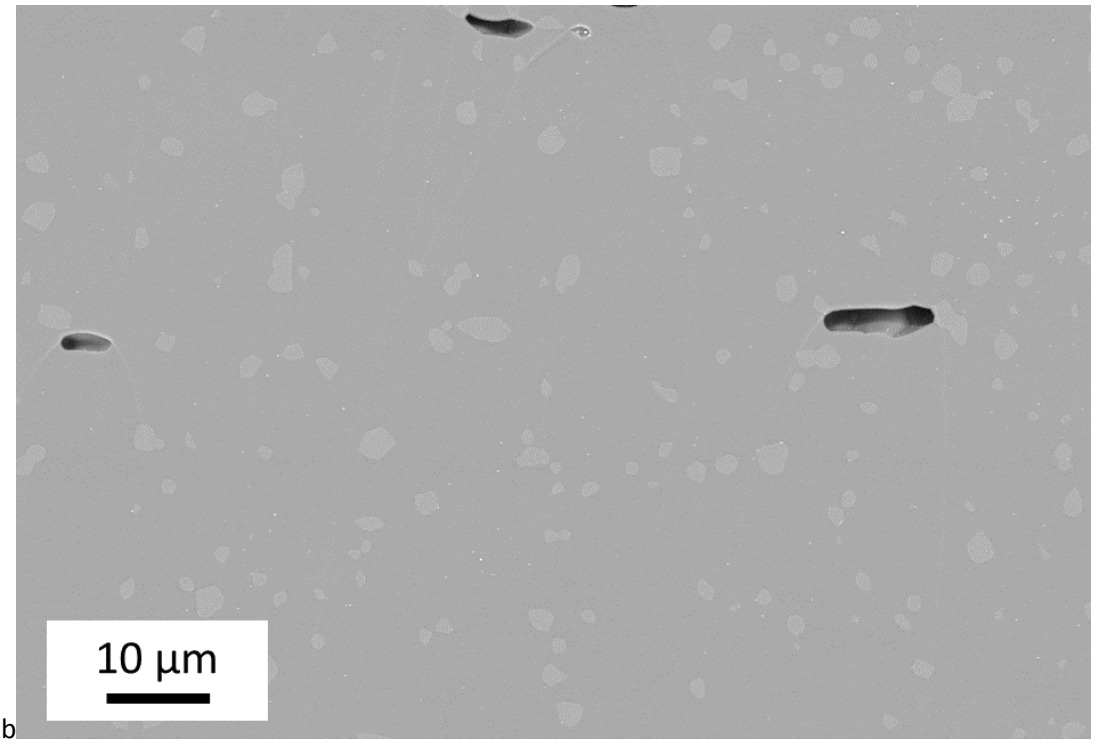

Fig 2b

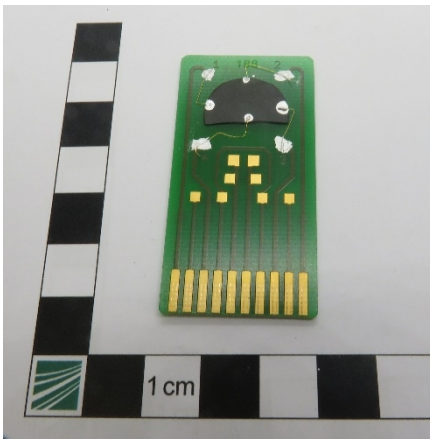

Fig 3a)

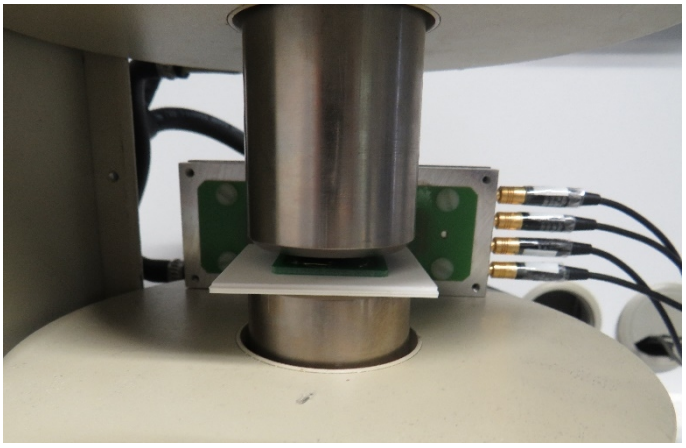

fig 3b)

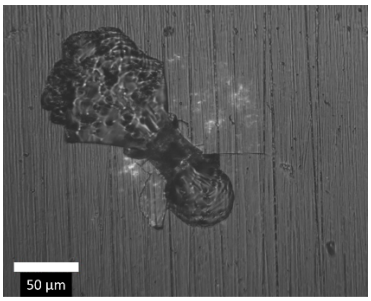

Fig 4a)

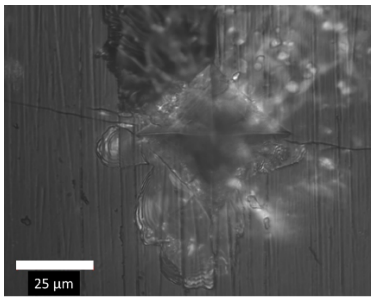

Fig 4b)

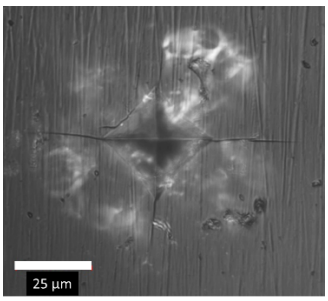

Fig 4c)

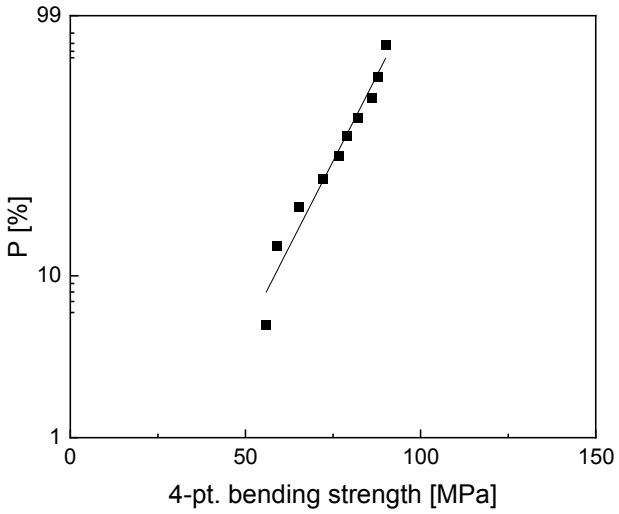

Fig 5

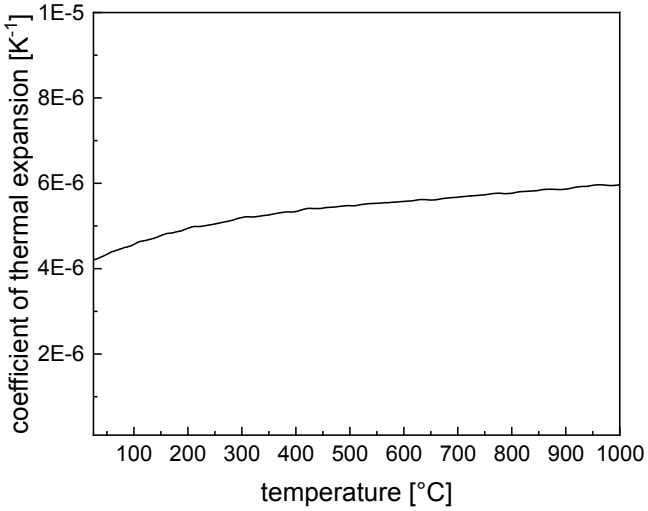

Fig 6

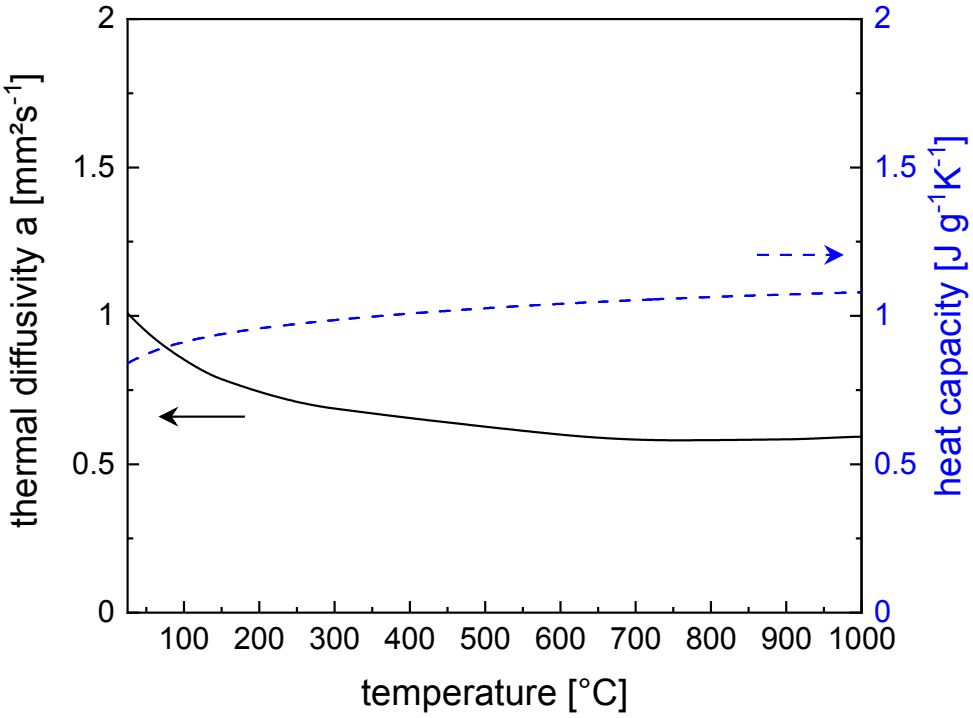

Fig 7

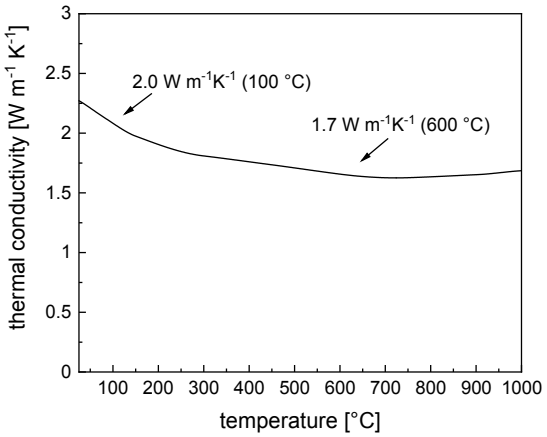

Fig 8

Figure 1 Phase diagram of CaO-Al_2O_3 system [1] with the phases C3A ($3CaO{\cdot}Al_2O_3$, $Ca_3Al_2O_6$), C12A7 ($12CaO{\cdot}7Al_2O_3$, $Ca_{12}Al_{14}O_{33}$), CA ($CaO{\cdot}Al_2O_3$, $CaAl_2O_4$), CA2 ($CaO{\cdot}2Al_2O_3$, $CaAl_6O_7$), and CA6 ($CaO{\cdot}6Al_2O_3$, $CaAl_{12}O_{19}$).

Figure 2 a) pattern of X-ray diffraction on a C12A7:e- ceramic with C12A7 main phase and impurities of $Ca_3Al_2O_6$ (C3A), b) SEM picture of polished surface of a sintered C12A7:e- ceramic with low pore content (dark holes), main phase of C12A7 and impurities of C3A grains (light grey).

Figure 3 Hall measurement: a) set-up of C12A7:e- sample contacted with van-der-Pauw geometry, b) sample set-up during measurement in the magnetic field.

Figure 4 Microscopic images of the indentation on the surface of polished C12A7:e- with a) HV5, b) HV1 and c) HV0.5.

Figure 5 Bending strength distribution of C12A7:e- ceramic.

Figure 6 Coefficient of thermal expansion (CTE) of C12A7:e- ceramic as function of the temperature.

Figure 8 Thermal conductivity (□) of C12A7:e- ceramic as function of the temperature.Figure 7 Thermal diffusivity (□) and heat capacity (cp) of C12A7:e- ceramic as function of the temperature.

References

[1] Zhang R, Mao H H, Taskinen P. Phase equilibria study and thermodynamic description of the BaO-CaO-Al_2O_3 system. J Am Ceram Soc. 2017; 100(6):2722-2731. https://doi.org/10.1111/jace.14793.

[2] Waetzig K, Rost A, Schilm J, Tajmar M, Michaelis A. Contacting Methods for C12A7 Electride Ceramic. J Ceram Sci Technol. 2019; 11(1):11-16. https://doi.org/10.4416/JCST2019-00032.

[3] Ebbinghaus S G, Krause H, Syrowatka F. Floating Zone Growth of Large and Defect-free $Ca_{12}Al_{14}O_{33}$ Single Crystals. Cryst Growth Des. 2013; 13:2990-2994. https://doi.org/10.1021/cg400406t.

[4] Kurashige K, Ueda S, Miyakawa M, Toda Y, Matsuishi S, Kim S, Hirano M, Hosono H. Growth of $12CaO{\cdot}7Al_2O_3$ single crystal with tetragonal symmetry by Czochralski method. Thin Solid Films. 2018; 516:5772-5776. https://doi.org/10.1016/j.tsf.2007.10.027.

[5] Kim SW, Matsuishi S, Miyakawa M, Hayashi K, Hirano M, Hosono H. Fabrication of room temperature-stable $12CaO \cdot 7Al_2O_3$ electride: a review. J Mater Sci: Mater Electron. 2007; 18:S5-S14. https://doi.org/10.1007/s10854-007-9183-y.

[6] Weber S, Schäfer S, Saccoccio M, Seidel K, Kohlmann H, Gläser R, Schunk SA. Mayenite-based electride C12A7e-: an innovative synthetic method via plasma arc melting. Mater Chem Front. 2020; 5:1301-1314. https://doi.org/10.1039/d0qm00688b.

[7] Feizi E & Ray AK. $12CaO{\cdot}7Al_2O_3$ Ceramic: A Review of the Electronic and Optoelectronic Applications in Display Devices. J Disp Technol. 2016; 12(5):451-459. https://doi.org/10.1109/JDT.2015.2496588.

[8] Jeevaratnam J, Glasser FP, Glasser LSD, Anion Substitution and Structure of $12CaO{\cdot}7Al_2O_3$. J Am Ceram Soc. 1964; 47(2):105-106. https://doi.org/10.1111/j.1151-2916.1964.tb15669.x.

[9] Lee DK, Kogel L, Ebbinghaus SG, Valov I, Wiemhoefer HD, Lerch M, Janek. Defect chemistry of the cage compound, $Ca_{12}Al_{14}O_{33-\delta}$—understanding the route from a solid electrolyte to a semiconductor and electride. J Phys Chem Chem Phys. 2009; 11:3105-3114. https://doi.org/10.1039/B818474G.

[10] Trofymluk O, Toda Y, Hosono H, Navrotsky A. Energetics of Formation and Oxidation of Microporous Calcium Aluminates: A New Class of Electrides and Ionic Conductors. Chem Mater. 2005; 17:5574-5579. https://doi.org/10.1021/cm051662w.

[11] Hosono H. Functioning of traditional ceramics $12CaO{\cdot}7Al_2O_3$ utilizing built-in nano-porous structure. Sci Technol Adv Mater. 2004; 5:409-416. https://doi.org/10.1016/j.stam.2004.01.012.

[12] Matsuishi S, Toda Y, Miyakawa M, Hayashi K, Kamiya T, Hirano M, Tanaka I, Hosono H. High-Density Electron Anions in a Nanoporous Single Crystal: $[Ca_{24}Al_{28}O_{64}]^{4+}(4e-)$. Science. 2003; 301:626-629. https://doi.org/10.1126/science.1083842.

[13] Toda Y, Kubota Y, Hirano M, Hirayama H, Hosono H. Surface of Room-Temperature-Stable Electride $[Ca_{24}Al_{28}O_{64}]^{4+}(e^-)_4$: Preparation and Its Characterization by Atomic-Resolution Scanning Tunneling Microscopy. ACS Nano. 2011; 5(3):1907-1914. https://doi.org/10.1021/nn102839k.

[14] Lobo RPSM, Bontemps N, Bertoni MI, Mason TO, Poeppelmeier KR, Freeman AJ, Park MS, Medvedeva JE. Optical Conductivity of Mayenite: From Insulator to Metal. J Phys Chem C. 2015; 119:8849-8856. https://doi.org/10.1021/acs.jpcc.5b00736.

[15] Kim SW, Hayashi K, Hirano M, Hosono H, Tanaka I. Electron Carrier Generation in a Refractory Oxide $12CaO{\cdot}7Al_2O_3$ by Heating in Reducing Atmosphere: Conversion from an Insulator to a Persistent Conductor. J Am Ceram Soc. 2006; 89(10):3294-3298. https://doi.org/10.1111/j.1551-2916.2006.01213.x.

[16] Zhao J, Zhang X, Liu H, Xiao Y, Jiang H, Zhang J, Synthesis and Characterization of $(Ca_{1-x}Sr_x)_{12}Al_{14}O_{33}$ Electrides. Cryst Res Technol. 2018; 53(1):1700201. https://doi.org/10.1002/crat.201700201.

[17] Li F, Zhang X, Liu H, Zhao J, Xiao Y, Feng Q, Zhang J. In situ synthesis of $[Ca_{24}Al_{28}O_{64}]^{4+}(4e-)$ electride ceramic from C12A7 + C3A mixture precursor. J Am Ceram Soc. 2019; 102:884-888. https://doi.org/10.1111/jace.16103.

[18] Xiao Y, Zhang X, Li R. $[Ca_{24}Al_{28}O_{64}]^{4+}(4e^-)$ are directly and quickly synthesized by self-reduction of $C_{12}H_{10}Ca_3O_{14} + Al_2O_3$ without any reducing agent. J Am Ceram Soc. 2020; 104(4): 1641-1648. https://doi.org/10.1111/jace.17558.

[19] Rudradawong C, Ruttanapun C. High temperature electrical and thermal properties of activated bamboo charcoal/C12A7 mayenite composite prepared by carbon diffusion process. Mater Chem Phys. 2019; 226:296-301. https://doi.org/10.1016/j.matchemphys.2019.01.028.

[20] Mackey J, Back T, Berger MH, Sayir A. Processing and thermal properties of mayenite electride. J Am Ceram Soc. 2021; 104(5): 2238-2249. https://doi.org/10.1111/JACE.17646.

[21] Shetty DK, Wright IG, Mincer PN, Clauer AH. Indentation fracture of WC-Co cermets. J Mater Sci. 1985; 20:1873-1882. https://doi.org/10.1007/BF00555296.